Check for updates

NANO · MICRO small
www.small-journal.com

Enhanced Performance of WS_2 Field-Effect Transistor through Mono and Bilayer h-BN Tunneling Contacts

*Nhat Anh Nguyen Phan, Hamin Noh, Jihoon Kim, Yewon Kim, Hanul Kim, Dongmok Whang, Nobuyuki Aoki, Kenji Watanabe, Takashi Taniguchi, and Gil-Ho Kim**

Transition metal dichalcogenides (TMDs) are of great interest owing to their unique properties. However, TMD materials face two major challenges that limit their practical applications: contact resistance and surface contamination. Herein, a strategy to overcome these problems by inserting a monolayer of hexagonal boron nitride (h-BN) at the chromium (Cr) and tungsten disulfide (WS_2) interface is introduced. Electrical behaviors of direct metal–semiconductor (MS) and metal–insulator–semiconductor (MIS) contacts with mono- and bilayer h-BN in a four-layer WS_2 field-effect transistor (FET) are evaluated under vacuum from 77 to 300 K. The performance of the MIS contacts differs based on the metal work function when using Cr and indium (In). The contact resistance is significantly reduced by approximately ten times with MIS contacts compared with that for MS contacts. An electron mobility up to ≈115 $cm^2 V^{-1} s^{-1}$ at 300 K is achieved with the insertion of monolayer h-BN, which is approximately ten times higher than that with MS contacts. The mobility and contact resistance enhancement are attributed to Schottky barrier reduction when h-BN is introduced between Cr and WS_2. The dependence of the tunneling mechanisms on the h-BN thickness is investigated by extracting the tunneling barrier parameters.

1. Introduction

In recent years, 2D materials have attracted significant attention owing to their unique properties and potential in various nanoelectronic applications such as field-effect transistor (FETs)[1–3] and logic circuits.[4,5] Among them, transition metal dichalcogenides (TMDs) have emerged as promising candidates for future nanoelectronics owing to their ultrathin structure, high intrinsic carrier mobility, and high on/off current ratio.[6–8] Among the known TMDs, tungsten disilfide (WS_2), which exhibits a transition from an indirect (1.4 eV) to a direct (2.1 eV) bandgap when cleaved into a monolayer,[9] is a promising candidate for electronic device applications. WS_2 also exhibits strong spin-orbit interactions, which enable spintronics and valleytronics.[10] Recently, several FETs fabricated with WS_2 as the channel material have performed low contact resistance and high field-effect mobility.[11–13]

A current challenge in achieving high-quality electronic devices is the contact resistance, which reduces the mobility as the Schottky barrier formation for charge injection significantly degrades the performance of devices. The formation of a large Schottky barrier and Fermi level pinning have been attributed to various metal–TMD interactions.[14,15] Therefore, an effective technique for reducing the contact resistance requires the formation of metal-insulator-semiconductor (MIS) contacts through the inclusion of an ultrathin tunneling insulator layer[16–21] at the metal–TMD interfaces. For instance, the performance of MoS_2 transistors has been enhanced with the incorporation of

N. A. N. Phan, H. Noh, J. Kim, Y. Kim, G.-H. Kim
Department of Electrical and Computer Engineering
Sungkyunkwan University (SKKU)
Suwon 16419, Republic of Korea
E-mail: ghkim@skku.edu

H. Kim, D. Whang, G.-H. Kim
Samsung-SKKU Graphene Centre
Sungkyunkwan Advanced Institute of Nanotechnology (SAINT)
Sungkyunkwan University (SKKU)
Suwon 16419, Republic of Korea

D. Whang
School of Advanced Materials Science and Engineering
Sungkyunkwan University (SKKU)
Suwon 16419, Republic of Korea

N. Aoki
Department of Materials Science
Chiba University
Chiba 263–8522, Japan

K. Watanabe
Research Center for Functional Materials
National Institute for Materials Science
1-1 Namiki, Tsukuba 305-0044, Japan

T. Taniguchi
International Center for Material Nano-Architectonics
National Institute for Materials Science
1-1 Namiki, Tsukuba 305-0044, Japan

The ORCID identification number(s) for the author(s) of this article can be found under https://doi.org/10.1002/smll.202105753.

DOI: 10.1002/smll.202105753

 © 2022 Wiley-VCH GmbH

a single-atom-thick h-BN as the tunneling layer. With this MIS structure, the Schottky barrier was considerably lowered from 158 to 31 meV, and a low contact resistance was achieved.[16] Recently, the contact resistance of *p*-type $MoTe_2$ was improved by covering it with monolayer WS_2 to form tunneling contacts.[22] Among these insulating layers, h-BN is more advantageous as it can hinder the interface states that cause Fermi level pinning by breaking the metal–TMD contacts and can reduce the work function of the transitional metal.[17]

In this study, we investigated the effect of the metal work function on the performance of MIS-structured few-layer WS_2 transistors using Cr and In as electrodes. We also compared the dicrect metal-semiconductor (MS) and MIS contacts of the devices by inserting mono and bilayer h-BN as tunneling barriers at the metal–WS_2 interfaces. The electrical characteristics of the few-layer WS_2 FETs were evaluated at temperatures ranging from 77 to 300 K. In particular, the MIS contacts of the Cr electrodes and the monolayer h-BN tunneling barrier showed remarkably high mobility. This improvement was attributed to the insertion of the single-atom-thick h-BN layer, which can lower the Schottky barrier height (SBH). Moreover, the electrical properties of MIS contacts with mono and bilayer h-BN thicknesses were compared to clarify the effect of h-BN on the device performance in terms of mobility, contact resistance, and tunneling barrier.

2. Results and Discussion

Figure 1a shows a schematic and false-colored scanning electron microscopy (SEM) image of the MIS-structured FET. The WS_2/h-BN heterostructure was transferred on a Si wafer covered with a 285-nm-thick SiO_2 film. WS_2 is the channel material of this device, whereas monolayer h-BN serves as a tunneling barrier between the metal and WS_2. Conventional mechanical exfoliation was performed to obtain multilayer WS_2 and monolayer h-BN flakes on SiO_2/Si substrates. The layers were then stacked using the dry transfer method in an argon (Ar) glove box, and electrodes were deposited using an electron-beam evaporator. The detailed fabrication process for the MIS-structured devices is illustrated in Figure S1 (Supporting Information). An optical microscope image of the MIS-structured FET with Cr electrodes is shown in Figure S2 (Supporting Information). The Raman spectra of the few-layer WS_2 and monolayer h-BN are shown in Figure 1b,c, respectively. The Raman spectrum of WS_2 exhibits two peaks: the E^1_{2g} peak at ≈349 cm^{-1}, which corresponds to the in-plane vibrational motion of atoms, and the A_{1g} peak at ≈416 cm^{-1}, which is attributed to the out-of-plane vibrational motion of the atoms. The findings thus confirm the presence of WS_2 in the exfoliated flakes.[23] By contrast, the Raman peak at ≈1370 cm^{-1} observed in Figure 1c is associated with the monolayer h-BN.[24] The thicknesses of WS_2 and h-BN were verified through atomic force microscopy (AFM), as shown in Figure 1d,e. The thickness of the WS_2 flake is 4.2 nm, confirming that it comprises four layers, whereas that of the h-BN flake is 0.51 nm, indicating that it is a monolayer.[17] The optical microscope image and AFM characterization of the device with In electrodes are demonstrated in Figure S3 (Supporting Information). In our study, two-terminal measurements were performed in a high-vacuum probe station at pressures below 20 mTorr and at various temperatures to study the electrical behavior of the MIS-structured device.

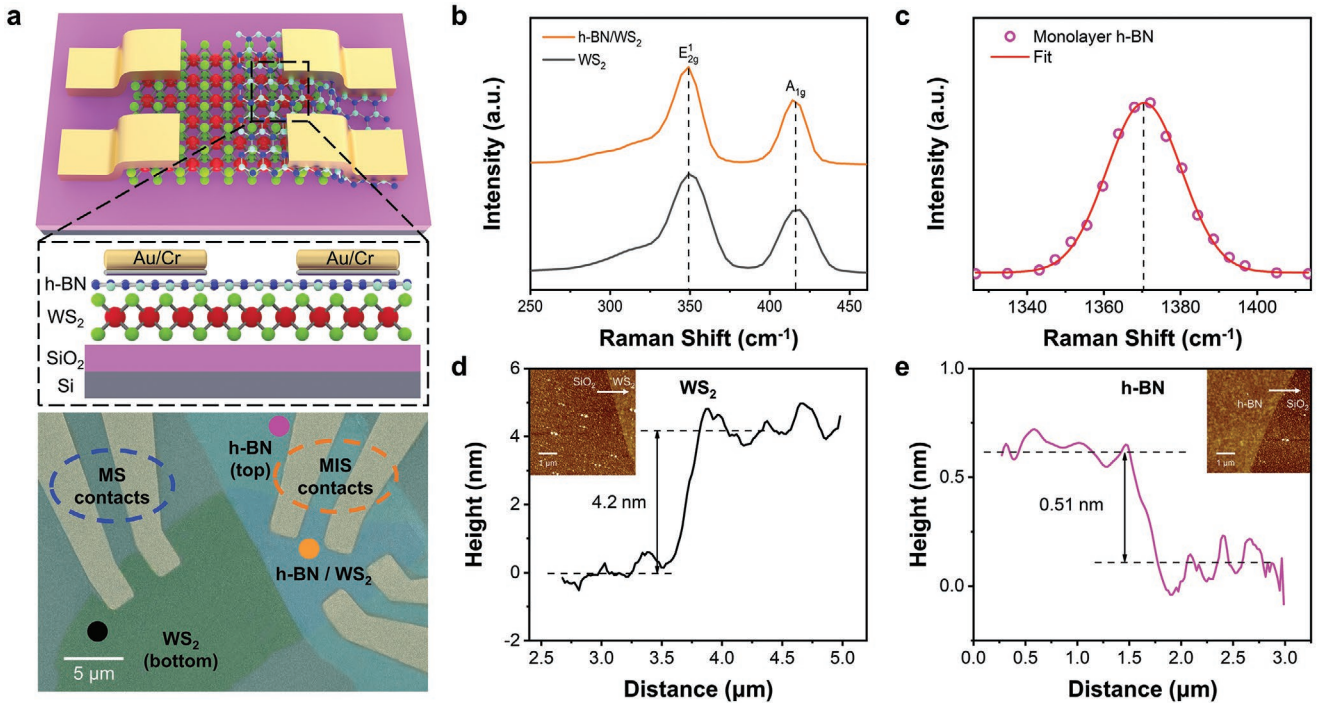

Figure 1. a) Schematic and false-color SEM image of the MIS-structured device with monolayer h-BN as the tunneling layer. b,c) Raman spectrum of the few-layer WS_2, h-BN/WS_2 heterostructure (b) and monolayer h-BN (c) corresponding to the three points in the false-color SEM image. d,e) AFM characterization of WS_2 and h-BN, respectively.

© 2022 Wiley-VCH GmbH

Figure 2 shows the two-terminal current–voltage (*I–V*) characteristics of the MS and MIS contacts with In and Cr at various gate biases. Based on the output characteristics of contacts with In electrodes presented in Figure 2a,b, the MS contacts exhibit ohmic behavior, whereas the MIS contacts show nonlinear behavior owing to the back-to-back Schottky diode-like structure. In contrast, when Cr is deposited as the electrodes, the MS contacts behave as Schottky contacts, indicating the formation of SBH between WS_2 and Cr (Figure 2c). Moreover, the MIS contacts behave as ohmic contacts with a higher current than that observed for the MS contacts, thus confirming their superior quality (Figure 2d). To explain these electrical characteristics, schematic band diagrams were plotted for each *I–V* curve. Assuming that the electron affinity of WS_2 (χ_{WS_2}) equals 4.4 eV,[25] the work functions of In (Φ_{In}) and Cr (Φ_{Cr}) are 4.12 and 4.5 eV, respectively.[26] When In is deposited onto WS_2, there is no oxidation or indium sulfide formation, distortions, or strain at the metal–semiconductor interface or within the 2D TMD materials; thus, defect-induced gap states can be avoided.[27] Ohmic-like transport is observed as a result of the strong density of in-gap states in the case of MS contacts with In electrodes.[28] However, when monolayer h-BN is inserted, there is a gap between In and WS_2, which results in SBH formation. Due to the occurrence of the SBH and the tunneling resistance of the h-BN, the performance of MIS contacts with In electrodes degrades and exhibits nonlinear behavior. In the case of Cr electrodes, the metal electron wave function penetrates the semiconductor at the MS junction, in accordance with the metal-induced gap states (MIGS) theory.[29,30] It charges the interface states of the semiconductor, forming a high Schottky barrier. When a thin h-BN layer is inserted, it attenuates the metal electron wave function prior to penetrating the semiconductor, which reduces the SBH. This single-atom-thick h-BN can improve the possibility of quantum tunneling. Another mechanism for the reduction in the SBH is the dipole formation at the h-BN/WS_2 or Cr/h-BN interfaces. The dipole at the interface of h-BN and WS_2 results from the difference in charge neutrality levels between h-BN and WS_2. The dipole at the Cr/h-BN interface is formed by the charge transfer between the Fermi level of Cr and charge neutrality of h-BN. Interfacial dipoles of opposite polarity prevent the intrinsic Fermi level from moving toward the charge neutrality level and neutralize the charges at the interface, leading to a reduction in the SBH.[21,31] Therefore, the MIS contacts with the Cr electrodes exhibit superior performance as opposed to the same contacts using In electrodes and the MS contacts with Cr electrodes. This observation is attributed to the removal of defect states at the MS interface.

The contact resistance of MIS contacts is mainly defined based on the tunneling resistance and Schottky barrier.[21,31–33] The SBH can be lowered by inserting an ultrathin h-BN, but this increases the tunneling resistance. A thick h-BN results in significant tunneling resistance, which decreases the current flow. To determine the optimal h-BN thickness, the device performance at different h-BN thicknesses was evaluated at various temperatures using the transfer curves and extracted SBHs presented in **Figure 3**. As illustrated in Figure 3a–c, the transfer curves of the device are typical of *n*-type WS_2. As the temperature decreases from 300 to 77 K, the current reduces significantly, which means that the decrease in the charge carrier is due to a reduction in the thermal energy. Moreover, with the insertion of h-BN, the on/off ratio of the device is improved compared to that of the MS contacts (Figure S4, Supporting Information). The superior performance of MIS contacts is a consequence of the reduced effects of tungsten and sulfide vacancies in WS_2 when an h-BN tunneling layer is inserted into the junction between Cr and WS_2.

To further understand the SBH of the contact, Arrhenius plots (Figure S5, Supporting Information) were studied and used to extract SBH (Φ_B). In a Schottky barrier device, the current in the subthreshold region is mainly defined by the thermally assisted tunneling and thermionic emission current.[34–36] In accordance with the thermionic theory, when the gate bias is below the flat-band voltage, the current can be described as follows

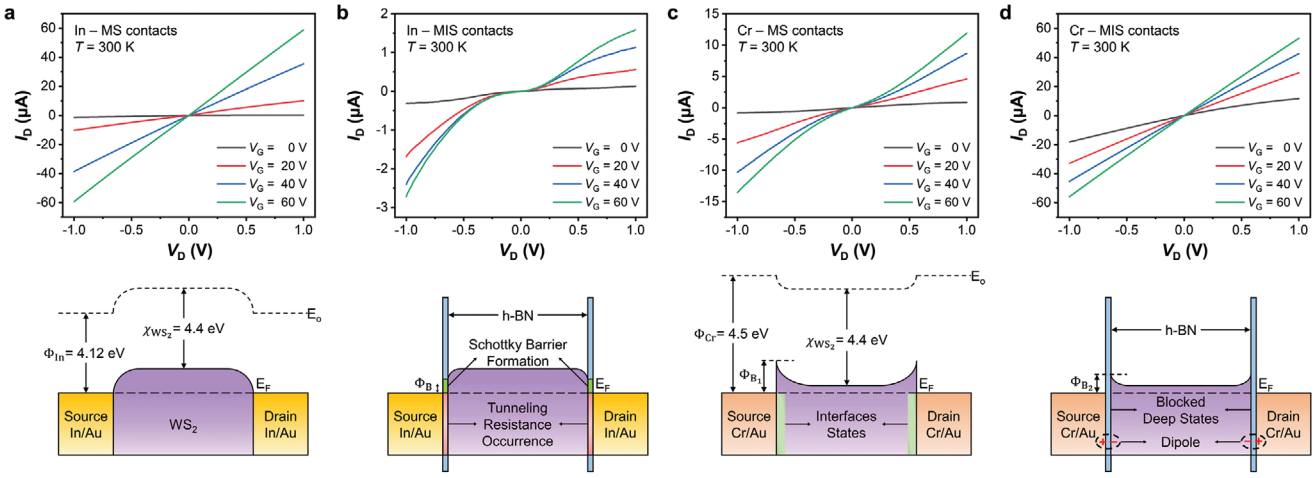

Figure 2. Output characteristics of the MS and MIS contacts with monolayer h-BN. a–d) Top panel: I_D–V_D curves of MS and MIS contacts with In (a,b) and Cr (c,d) electrodes at 300 K under different gate biases, respectively. Bottom panel: energy band diagrams for each type of contact. In the case of In electrodes, the MS contacts behave as ohmic contacts whereas the MIS contacts show nonlinear behavior owing to the SBH formation and tunneling resistance of the h-BN. In the case of Cr electrodes, the SBH is significant because of the MIGS penetration, but when a monolayer h-BN is inserted, the SBH is reduced because of the minimization of MIGS penetration and dipole formation.

© 2022 Wiley-VCH GmbH

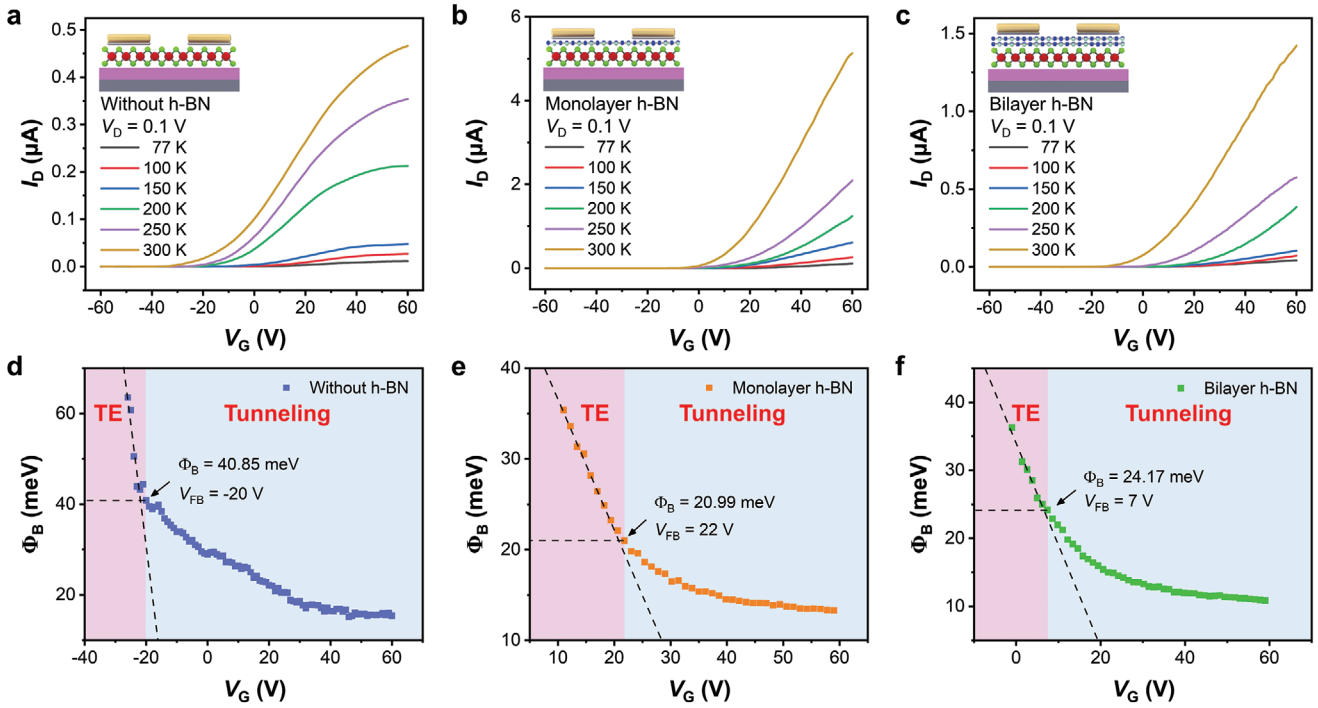

Figure 3. a–c) Temperature dependence of transfer characteristics of MS and MIS contacts with mono and bilayer h-BN. The transfer curves were recorded by sweeping the gate voltage while applying a fixed drain voltage V_D = 0.1 V and measuring the drain current at different temperatures varying from 77 to 300 K. d–f) Extracted SBHs for different back gate biases when h-BN comprises zero, one, and two layers, respectively. The pink region indicates that the thermionic emission current is dominant, whereas the thermally assisted tunneling current dominates the blue region.

$$I_D = A^*_{2d}\, T^{3/2} exp\left(\frac{q\Phi_B}{k_B T}\right)\left[1 - exp\left(-\frac{qV_D}{k_B T}\right)\right] \quad (1)$$

where I_D is the current through the device, A^*_{2d} is the 2D equivalent Richardson constant, T is the absolute temperature, q is the charge of an electron, k_B is the Boltzmann constant, and V_D is the applied drain-to-source bias of 0.1 V.[19,35,36] When the gate bias (V_G) is smaller than the flat-band voltage (V_{FB}), the current through the device is dominated by the thermionic emission current. When V_G is higher than V_{FB}, both components contribute to the current flow, which is not considered in thermionic emission theory. This results in a nonlinear behavior. When V_G equals V_{FB}, Φ_B can be accurately extracted from the slope, because the thermally assisted tunneling current becomes negligible. Therefore, to accurately determine Φ_B based on the thermionic emission theory and diode (Equation 1), Φ_B must be determined under the flat-band voltage condition ($V_G = V_{FB}$). Φ_B was initially plotted as a function of the gate voltage for different h-BN thicknesses, as shown in Figure 3d–f. As V_G increases above V_{FB}, the tunneling current component dominates, and the plot deviates from its linear relationship. Therefore, the accurate Φ_B value obtained under flat-band voltage conditions for the MS contacts is 40.85 meV (Figure 3d). The Φ_B values of the MIS contacts are 20.99 and 24.17 meV for the mono and bilayer h-BN, respectively, which are twice lower than those of the MS contacts (Figure 3e,f). These findings indicate that the insertion of h-BN reduces the SBH of the device.

For an in-depth comparison of the electrical properties of MS and MIS contacts, the field-effect mobility μ_{FE} was obtained using the following equation:

$$\mu_{FE} = \left(\frac{L}{WC_{ox}}\right)\frac{g_m}{V_D} \quad (2)$$

where C_{ox} is the oxide capacitance of 12.1 nF cm^{-2}, W and L are the channel width and length of the device, respectively, g_m is the transconductance, defined as dI_D/dV_G and V_D is the applied drain voltage of 0.1 V. As illustrated in **Figure 4**a, the mobilities of the contacts with mono and bilayer h-BN were extracted from 77 to 300 K. The temperature dependence of the mobility can be described by the power law $\mu_{FE} \approx T^{\gamma}$, which indicates a difference in the electron transport mechanism. The mobility curves of all the contacts show similar trends and a consistent dependence on temperature. The value of the exponent γ was determined to be 1.87 for the MS contacts, 2.79 and 2.75 for the MIS contacts with mono and bilayer h-BN, respectively. Interestingly, the mobility of the MIS contacts with monolayer h-BN was approximately ten times and three times higher than the MS and MIS contacts with bilayer h-BN, respectively, at every investigated temperature. The highest mobility of the MIS contacts with monolayer h-BN was 115.69 cm^2 V^{-1} s^{-1} at 300 K. Moreover, In, a metal with a low work function, was used to investigate the effect of the work function of metals on the performance of the device (Figure S6a,b, Supporting Information). The device with In shows a nonlinear behavior due to its back-to-back Schottky diode-like structure, which results in a low

© 2022 Wiley-VCH GmbH

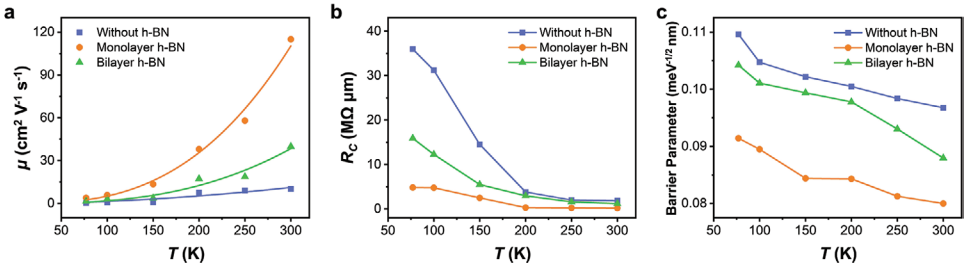

Figure 4. Temperature dependence of a) mobility, b) contact resistance, and c) DT barrier of the device with MS and MIS contacts with mono and bilayer h-BN.

mobility of ≈1.44 $cm^2\ V^{-1}\ s^{-1}$ at 300 K (Figure S6d, Supporting Information). To understand the change in contact resistance due to the insertion of h-BN, the contact resistance owing to the MS and MIS contacts was evaluated using the Y-function (Ghibaudo) method,[37,38] as described in detail in the Supporting Information. By using this method, the contact resistance can be calculated accurately from two-terminal electrical measurements, as presented in Figure 4b. With monolayer h-BN, the contact resistance significantly reduced from 1.83 to 0.18 MΩ μm and from 35.96 to 4.82 MΩ μm at 300 and 77 K, respectively. In the case of MS contacts, the contact resistance was dominated by the Schottky barrier. Introducing an ultrathin h-BN as a tunneling layer can reduce the Schottky barrier while maintaining low tunneling resistance owing to the atomic thickness. However, the contact resistance for the bilayer h-BN MIS contacts varied in the range of 1.19–15.89 MΩ μm when the temperature decreased from 300 to 77 K; the contact resistance was larger than that observed for monolayer h-BN. The change in the contact resistance was ascribed to the increase in tunneling resistance. In the case of thick h-BN layers, tunneling resistance plays a significant role and consequently dominates the measured contact resistance. Therefore, the monolayer h-BN is the most appropriate for MIS contacts to enhance the electrical properties of the devices.

Moreover, to gain further insight into the transport characteristics of the four-layer WS_2 with the MS and MIS contacts, we used the direct tunneling (DT) and Fowler–Nordheim tunneling (F–N) models. Although electrons are expected to be thermally excited to overcome the Schottky barrier owing to the thermionic emission mechanism, DT is more dominant at lower temperatures for an ultrathin barrier. In F–N, which mainly occurs at high biases, electrons can tunnel through a triangular shape of the barrier.[39] DT can be described as[40,41]

$$I_D = \frac{Aq^2V\sqrt{2m^*\Phi_B}}{h^2d}\,exp\left(-\frac{4\pi d\sqrt{2m^*\Phi_B}}{h}\right) \quad (3)$$

where A is the electrical contact area, d *is* the barrier width, h is Planck's constant, m* is the effective mass of an electron in the WS_2 flake (0.33 m_o,[42] where m_o is the rest mass), and Φ_B is the SBH.

F–N is described as[40,41]

$$I_D = \frac{Aq^3m_oV^2}{8\pi h\Phi_B d^2m^*}\,exp\left(-\frac{8\pi\sqrt{2m^*}\Phi_B^{3/2}d}{3hqV}\right) \quad (4)$$

All the contacts exhibit a logarithmic relationship, which indicates that DT becomes significant in the devices, as shown in Figure S7 (Supporting Information). DT illustrates a linear behavior when $\ln(I_D/V_D^2)$ is plotted as a function of $\ln(1/V_D)$ (Figure S7d–f, Supporting Information). In addition, there is no indication of the F–N mechanism, because F–N generally occurs at higher bias voltages. By following Equation 3, the barrier parameter ($d\sqrt{\Phi_B}$) can be determined from the fitting equation for DT (see Supporting Information). The tunneling barrier heights of the MS and MIS contacts are demonstrated in Figure 4c. The barrier parameter of the MS contacts was in the range of 0.10–0.11 $meV^{-1/2}$ nm when the temperature decreased from 300 to 77 K. The barrier parameter of the MIS contacts was lower than that of the MS contacts; it varied in the range of 0.08–0.09 and 0.09–0.10 $meV^{-1/2}$ nm for mono and bilayer h-BN, respectively, when the temperature decreased from 300 to 77 K. From the above result, it is evident that the barrier parameter of the tunneling contacts is below that of the WS_2 direct contacts at all temperatures, signifying that the insertion of h-BN prevents the formation of an interfacial barrier layer at the junction and lowers the SBH. However, the tunneling barrier of bilayer h-BN is higher than that of the monolayer h-BN, because a thicker h-BN yields a more significant barrier and tunneling resistance. Therefore, monolayer h-BN is the most appropriate thickness to achieve a high-performance MIS-structured device.

To further investigate the effects of h-BN, we fabricated MIS-structured devices with Cu (Φ = 4.7 eV) and Pd (Φ = 5.12 eV). The electrical characteristics of these devices are presented in Figure S8 (Supporting Information). **Figure 5** demonstrates a comparison of the extracted SBHs (Figure 5a) and contact resistance (Figure 5b) of the MS and MIS contacts with different metal electrodes. In the case of Cr, Cu, or Pd, the SBH is reduced by the insertion of h-BN owing to the minimization of MIGS penetration and dipole formation as discussed above, which results in a lower contact resistance of MIS contacts compared to MS contacts. On the other hand, when In is used as an electrode, the electrical behavior of the MS and MIS contacts is opposite to that of the other metal electrodes because of the SBH and h-BN tunneling resistance. Therefore, depending on the metal work function, the MIS strategy can bring benefits or drawbacks to the contact quality. The existence of an additional insulating layer at the contact may not be favorable because it provides an additional barrier and tunneling resistance.

© 2022 Wiley-VCH GmbH

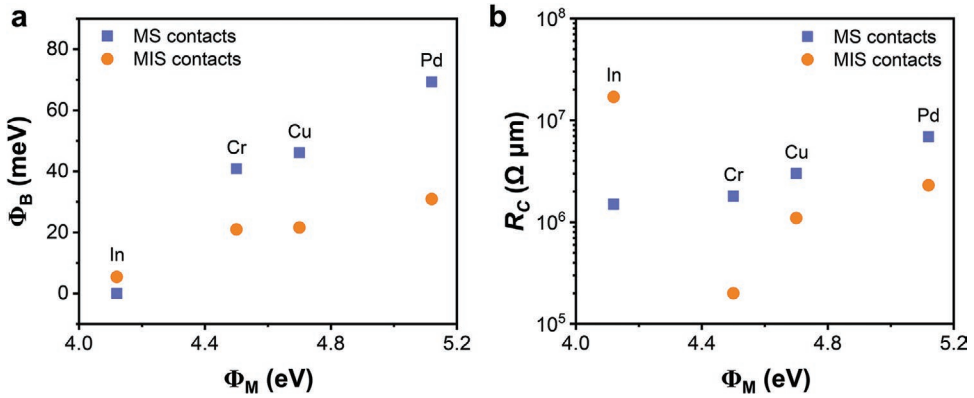

Figure 5. Comparison of a) SBHs and b) contact resistance of the MS and MIS contacts as a function of metal work function.

3. Conclusion

In summary, we performed a comprehensive study on improving the electron mobility and contact resistance of four-layer WS_2 transistors by introducing monolayer h-BN as a tunneling layer between WS_2 and Cr. Because the improvement of MIS-structured devices is dependent on SBH reduction, we studied the related mechanism and calculated the SBH for each contact. In addition, we compared the barrier parameters of the MS and MIS contacts with mono and bilayer h-BN to explain how h-BN improves the device performance. Our study provides an opportunity to understand the mechanism of SBH reduction, which can support the investigation of the electrical properties of TMD materials, in addition to improving the fundamental transport properties and enabling the realization of novel electronic device applications.

4. Experimental Section

Mono and Bilayer Tunneling Barrier WS_2 FET Fabrication: During the preparation, 1 cm^2 SiO_2 (285 nm)/Si substrates were cleaned with an ultrasonic cleaning machine for 10 min in acetone and isopropyl alcohol, respectively. Multilayer WS_2 flakes were mechanically exfoliated from bulk crystals (2D Semiconductors, Inc.) onto a SiO_2/Si substrate. By using an exfoliation machine designed in the laboratory, the temperature, pressing force, and exfoliation time were controlled appropriately to obtain monolayer and bilayer h-BN from bulk crystals grown at the National Institute of Materials Science and Technology in Japan. The thicknesses of WS_2 and h-BN were determined using an optical microscope, and then verified through atomic force microscopy. The dry transfer method was followed in an Ar glove box to stack the WS_2/h-BN heterostructure on the SiO_2/Si substrate. The next step was patterning via electron-beam lithography and deposition via electron-beam evaporation (Korea Vacuum Tech. KVT-2004). The chosen metals for the electrodes were In or Cr and Au with a 10 nm:30 nm ratio. After device fabrication, the sample was annealed at 150 °C in Ar gas for 2 h (Nextron RTP-1200).

Device Characterization: Raman spectroscopy was performed to characterize the flakes by using a 532 nm laser under ambient conditions. The thicknesses of the WS_2 and h-BN flakes were verified using AFM. The electrical properties of the device were evaluated under vacuum using a Keithley 4200-SCS parameter analyzer. The temperature was controlled using liquid nitrogen and a Hot Chuck controller MST-1000H. The electrical data of the device was recorded using the Star Sagittarius program.

Supporting Information

Supporting Information is available from the Wiley Online Library or from the author.

Acknowledgements

This work was supported by the National Research Foundation of Korea (NRF) grant funded by the Korean government (MSIT) (No. 2019R1A2C2088719 and 2021K2A9A2A08000168). This work was supported by the JSPS KAKENHI Grant Nos. 18H0812 and 20J20052, JSPS Bilateral Joint Research with NRF, Chiba University VBL project, and Iketani Science and Technology Foundation. K.W. and T.T. acknowledge support from the Elemental Strategy Initiative conducted by the MEXT, Japan, Grant Number JPMXP0112101001, JSPS KAKENHI Grant Numbers JP20H00354 and the CREST (JPMJCR15F3), JST.

Conflict of Interest

The authors declare no conflict of interest.

Data Availability Statement

Research data are not shared.

Keywords

2D transition metal dichalcogenides, contact resistance, mono and bilayer h-BN, tunneling barrier, Schottky barrier

Received: September 20, 2021
Revised: December 20, 2021
Published online:

[1] B. Radisavljevic, A. Radenovic, J. Brivio, V. Giacometti, A. Kis, *Nat. Nanotechnol.* **2011**, *6*, 147.
[2] Y. S. Shin, K. Lee, Y. R. Kim, H. Lee, I. M. Lee, W. T. Kang, B. H. Lee, K. Kim, J. Heo, S. Park, Y. H. Lee, W. J. Yu, *Adv. Mater.* **2018**, *30*, 1704435.
[3] M. A. Khan, S. Rathi, C. Lee, D. Lim, Y. Kim, S. J. Yun, D. H. Youn, G. H. Kim, *ACS Appl. Mater. Interfaces* **2018**, *10*, 23961.

© 2022 Wiley-VCH GmbH

[4] E. Liu, Y. Fu, Y. Wang, Y. Feng, H. Liu, X. Wan, W. Zhou, B. Wang, L. Shao, C. H. Ho, Y. S. Huang, Z. Cao, L. Wang, A. Li, J. Zeng, F. Song, X. Wang, Y. Shi, H. Yuan, H. Y. Hwang, Y. Cui, F. Miao, D. Xing, *Nat. Commun.* **2015**, *6*, 6991.
[5] B. Radisavljevic, M. B. Whitwick, A. Kis, *ACS Nano* **2011**, *5*, 9934.
[6] H. J. Chuang, X. Tan, N. J. Ghimire, M. M. Perera, B. Chamlagain, M. M. C. Cheng, J. Yan, D. Mandrus, D. Tománek, Z. Zhou, *Nano Lett.* **2014**, *14*, 3594.
[7] B. Radisavljevic, A. Kis, *Nat. Mater.* **2013**, *12*, 815.
[8] D. Qu, X. Liu, M. Huang, C. Lee, F. Ahmed, H. Kim, R. S. Ruoff, J. Hone, W. J. Yoo, *Adv. Mater.* **2017**, *29*, 1606433.
[9] H. Zeng, G. B. Liu, J. Dai, Y. Yan, B. Zhu, R. He, L. Xie, S. Xu, X. Chen, W. Yao, X. Cui, *Sci. Rep.* **2013**, *3*, 1608.
[10] L. Y. Yang, N. A. Sinitsyn, W. B. Chen, J. T. Yuan, J. Zhang, J. Lou, S. A. Crooker, *Nat. Phys.* **2015**, *11*, 830.
[11] Y. Cui, R. Xin, Z. Yu, Y. Pan, Z. Y. Ong, X. Wei, J. Wang, H. Nan, Z. Ni, Y. Wu, T. Chen, Y. Shi, B. Wang, G. Zhang, Y. W. Zhang, X. Wang, *Adv. Mater.* **2015**, *27*, 5230.
[12] H. M. Khalil, M. F. Khan, J. Eom, H. Noh, *ACS Appl. Mater. Interfaces* **2015**, *7*, 23589.
[13] M. W. Iqbal, M. Z. Iqbal, M. F. Khan, M. A. Shehzad, Y. Seo, J. H. Park, C. Hwang, J. Eom, *Sci. Rep.* **2015**, *5*, 10699.
[14] A. Allain, J. Kang, K. Banerjee, A. Kis, *Nat. Mater.* **2015**, *14*, 1195.
[15] S. L. Li, K. Komatsu, S. Nakaharai, Y. F. Lin, M. Yamamoto, X. Duan, K. Tsukagoshi, *ACS Nano* **2014**, *8*, 12836.
[16] J. Wang, Q. Yao, C. W. Huang, X. Zou, L. Liao, S. Chen, Z. Fan, K. Zhang, W. Wu, X. Xiao, C. Jiang, W. W. Wu, *Adv. Mater.* **2016**, *28*, 8302.
[17] X. Cui, E. M. Shih, L. A. Jauregui, S. H. Chae, Y. D. Kim, B. Li, D. Seo, K. Pistunova, J. Yin, J. H. Park, H. J. Choi, Y. H. Lee, K. Watanabe, T. Taniguchi, P. Kim, C. R. Dean, J. C. Hone, *Nano Lett.* **2017**, *17*, 4781.
[18] H. N. Jaiswal, M. Liu, S. Shahi, S. Wei, J. Lee, A. Chakravarty, Y. Guo, R. Wang, J. M. Lee, C. Chang, Y. Fu, R. Dixit, X. Liu, C. Yang, F. Yao, H. Li, *Adv. Mater.* **2020**, *32*, 2002716.
[19] T. S. Ghiasi, J. Quereda, B. J. V. Wees, *2D Mater.* **2019**, *6*, 015002.
[20] A. Dankert, L. Langouche, M. V. Kamalakar, S. P. Dash, *ACS Nano* **2014**, *8*, 476.
[21] S. Lee, A. Tang, S. Aloni, H. S. Wong, *Nano Lett.* **2016**, *16*, 276.
[22] J. Kim, A. Venkatesan, H. Kim, Y. Kim, D. Whang, G. H. Kim, *Adv. Sci.* **2021**, *8*, 2100102.
[23] A. Berkdemir, H. R. Gutierrez, A. R. Botello-Mendez, N. Perea-Lopez, A. L. Elias, C. I. Chia, B. Wang, V. H. Crespi, F. Lopez-Urias, J. C. Charlier, H. Terrones, M. Terrones, *Sci. Rep.* **2013**, *3*, 1755.
[24] R. V. Gorbachev, I. Riaz, R. R. Nair, R. Jalil, L. Britnell, B. D. Belle, E. W. Hill, K. S. Novoselov, K. Watanabe, T. Taniguchi, A. K. Geim, P. Blake, *Small* **2011**, *7*, 465.
[25] W. S. Hwang, M. Remskar, R. Yan, V. Protasenko, K. Tahy, S. D. Chae, P. Zhao, A. Konar, H. Xing, A. Seabaugh, D. Jena, *Appl. Phys. Lett.* **2012**, *101*, 013107.
[26] J. Peisner, P. Roboz, P. B. Barna, *Phys. Stat. Sol.* **1971**, *4*, K187.
[27] Y. Wang, J. C. Kim, R. J. Wu, J. Martinez, X. Song, J. Yang, F. Zhao, A. Mkhoyan, H. Y. Jeong, M. Chhowalla, *Nature* **2019**, *568*, 70.
[28] B. K. Kim, T. H. Kim, D. H. Choi, H. Kim, K. Watanabe, T. Taniguchi, H. Rho, J. J. Kim, Y. H. Kim, M. H. Bae, *npj 2D Mater. Appl.* **2021**, *5*, 9.
[29] V. Heine, *Phys. Rev.* **1965**, *138*, A1689.
[30] J. Tersoff, *Phys. Rev. Lett.* **1984**, *52*, 465.
[31] J. Hu, A. Nainani, Y. Sun, K. C. Saraswat, H. S. P. Wong, *Appl. Phys. Lett.* **2011**, *99*, 252104.
[32] U. Chandni, K. Watanabe, T. Taniguchi, J. P. Eisenstein, *Nano Lett.* **2016**, *16*, 7982.
[33] S. McDonnell, B. Brennan, A. Azcatl, N. Lu, H. Dong, C. Buie, J. Kim, C. L. Hinkle, M. J. Kim, R. M. Wallace, *ACS Nano* **2013**, *7*, 10354.
[34] S. Das, H. Y. Chen, A. V. Penumatcha, J. Appenzeller, *Nano Lett.* **2013**, *13*, 100.
[35] M. Farmanbar, G. Brocks, *Phys. Rev. B* **2015**, *91*, 161304.
[36] W. Wang, Y. Liu, L. Tang, Y. Jin, T. Zhao, F. Xiu, *Sci. Rep.* **2014**, *4*, 6928.
[37] R. Dagan, Y. Vaknin, A. Henning, J. Y. Shang, L. J. Lauhon, Y. Rosenwaks, *Appl. Phys. Lett.* **2019**, *114*, 101602.
[38] G. Ghibaudo, *Electron. Lett.* **1988**, *24*, 543.
[39] F. Ahmed, M. S. Choi, X. Liu, W. J. Yoo, *Nanoscale* **2015**, *7*, 9222.
[40] S. Das, A. Prakash, R. Salazar, J. Appenzeller, *ACS Nano* **2014**, *8*, 1681.
[41] J. R. Duran Retamal, D. Periyanagounder, J. J. Ke, M. L. Tsai, J. H. He, *Chem. Sci.* **2018**, *9*, 7727.
[42] J. Chang, L. F. Register, S. K. Banerjee, *J. Appl. Phys.* **2014**, *115*, 084506.

© 2022 Wiley-VCH GmbH